การศึกษาเชิงทฤษฎีของการถ่ายโอนโปรตอนภายในโมเลกุลของฟลาโวนอลด้วยทฤษฎีเดนซิตีฟังก์ชันนัล

Theoretical Study of Intramolecular Proton Transfer in Flavonols with Density Functional Theory

ขจัดภัย ทิพยผ่อง และ ณัฐวิศิษฏ์ ยะสารวรรณ*

Khajadpai Thipyapong and Nuttawisit Yasarawan*

ภาควิชาเคมี คณะวิทยาศาสตร์ มหาวิทยาลัยบูรพา

Chemistry Department, Faculty of Science, Burapha University

Received : 27 April 2018

Accepted : 18 June 2018

Published online : 25 June 2018

บทคัดย่อ

ทำการศึกษาปฏิกิริยาการถ่ายโอนโปรตอนภายในโมเลกุลของฟลาโวนอลสี่ชนิด ได้แก่ แคมพ์เฟอรอล มอริน มอริน-5*-ซัลโฟเนต และมอริน-7-โอ-ซัลเฟต ในสารละลายน้ำ ด้วยระเบียบวิธีทฤษฎีเดนซิตีฟังก์ชันนัล ภายใต้แบบจำลองโพราไรซาเบิลคอนตินิวอัม ระดับของทฤษฎีที่ใช้คือ B3LYP/6-311++G(d,p) และ CAM-B3LYP/6-311++G(d,p) สถานะทรานซิชันของปฏิกิริยาถูกคำนวณด้วยวิธีคิวเอสทีทู สำหรับฟลาโวนอลทุกชนิดที่ทดสอบพบว่ารูปแบบปกติมีความเสถียรสูงกว่ารูปแบบสวิทเทอร์ไอออนเป็นอย่างมาก เนื่องจากรูปแบบปกติมีการกระจายความหนาแน่นของอิเล็กตรอนภายในโมเลกุลที่สม่ำเสมอ ศักยภาพในการถ่ายโอนโปรตอนภายในโมเลกุลของฟลาโวนอลขึ้นอยู่กับความแข็งแรงของพันธะไฮโดรเจนภายในโมเลกุลและผลกระทบทางอิเล็กตรอนของหมู่แทนที่ โดยข้อมูลทางอุณหพลศาสตร์และจลนศาสตร์ชี้ให้เห็นว่าปฏิกิริยาการถ่ายโอนโปรตอนภายในโมเลกุลเกิดขึ้นได้ง่ายที่สุดและยากที่สุดในกรณีของมอริน-7-โอ-ซัลเฟตและแคมพ์เฟอรอล ตามลำดับ

คำสำคัญ : ทฤษฎีเดนซิตีฟังก์ชันนัล, พีซีเอ็ม, การถ่ายโอนโปรตอน, ฟลาโวนอล

Abstract

Intramolecular proton transfer (IPT) reactions of four flavonols. i.e. kaempferol, morin, morin-5*-sulfonate and morin-7-O-sulfate in aqueous solution have been investigated using density functional methods with under polarizable continuum model (PCM). The levels of theory used were B3LYP/6-311++G(d,p) and CAM-B3LYP/6-311++G(d,p). Transition states of reactions were calculated using the QST2 method. For all flavonols tested, the normal form is much more stable than its respective zwitterionic form, due to the marked uniformity of electron density distribution in the molecular structure of the former. The potential for each flavonol to undergo IPT depends considerably on either the strength of intramolecular hydrogen bonding or electronic effect of substituents. The computed thermodynamic and kinetic data altogether manifest that the most and the least favorable IPT reactions belong to morin-7-O-sulfate and kaempferol, respectively.

Keywords : Density Functional Theory, PCM, proton transfer, flavonols

***Corresponding author. E-mail** : nuttawisit@buu.ac.th

Introduction

Flavonols are a group of phytonutrients belonging to the flavonoid family which play considerable roles in the development of pharmaceuticals, foods and healthcare products. Among several types of flavonols, kaempferol-based compounds and their metal chelates have been reported as exhibiting diverse medicinal benefits such as antimicrobial, antiviral, cardiovascular protective, anticancer, antidiabetic and antioxidant activities (Calderon-Montaño *et al*., 2011; Panhwar & Memon, 2011; Alkhamees, 2013; Chen & Chen, 2013; Pieniazek *et al*., 2014). The antioxidant properties of most flavonols including kaempferol are primarily based on their ability to scavenge reactive oxygen and nitrogen radical species which are the cause of oxidative stress in humans (Chen *et al*., 1990; Seyoum *et al*., 2006; Markovic *et al*., 2012). As the scavenging activity relies considerably on the potential of flavonol molecule to donate hydrogen atom to the reactive radical species, the mechanisms by which the hydrogen atoms are released from the hydroxyl groups in flavonols have been of fundamental interest in the pharmaceutical context (Markovic *et al*., 2012). One of the most well-known hydrogen-relocating phenomena feasible in flavonols is intramolecular proton transfer (IPT) (McMorrow & Kasha, 1984; Sengupta et al., 2015).

Scheme 1. Kaempferol-based compounds for this study.

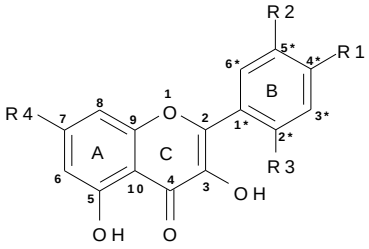

Compound	R1	R2	R3	R4
Kaempferol	—OH	—H	—H	—OH
Morin	—OH	—H	—OH	—OH
Morin-5*-sulfonate	—OH	$-SO_3^-$	—OH	—OH
Morin-7-O-sulfate	—OH	—H	—OH	$-OSO_3^-$

All kaempferol-based compounds shown in Scheme 1 bear the same 3-hydroxyflavone skeleton, consisting of a chromone moiety which is a benzene ring (ring A) fused with a pyrone ring (ring C). Ring C has a phenyl ring (ring B) substituted specifically at position C2. In each kaempferol-based molecule, the C3 hydroxyl proton could be presumably relocated to the nearest carbonyl oxygen atom, yielding zwitterionic form. It would be useful in terms of pharmaceutical development to gain a profound understanding in the effect of substituents added to the kaempferol skeleton on the potential of molecule to undergo the IPT reaction. Previously, apart from a variety of experimental techniques, density functional theory (DFT) methods have been widely used in describing the hydrogen transfer behavior of several organic compounds including flavonoids both in ground and excited states (Doroshenko *et al*., 2000; Georgieva *et al*., 2007; Yasarawan *et al*., 2014). In the present study, the stable geometries

in water of various normal and zwitterionic species of four kaempferol-based compounds as depicted in Scheme 1 have been determined by means of full geometry optimization with DFT methods under polarizable continuum model. The thermodynamic and kinetic driving forces for each compound to undergo either conformational change or IPT have been evaluated on the basis of computational thermodynamic and kinetic parameters of reactions.

Methods

The ground-state geometries of all studied compounds were fully optimized with the *Gaussian 16* program package (Frisch *et al*., 2016) using DFT methods. Either the hybrid exchange-correlation functional B3LYP (Lee *et al*., 1988; Becke, 1993) or the long-range-corrected functional CAM-B3LYP (i.e., B3LYP equipped with coulomb-attenuating method to account for the long-range HF exchange interactions) (Yanai *et al*., 2004) was used in the calculations. B3LYP has become a standard density functional used in the DFT investigation of both molecular geometries and electronic properties of several organic molecules including flavonoids. In a number of recent works, CAM-B3LYP has been reported as being more effective in predicting electronic properties than its predecessor B3LYP (Jacquemin *et al*., 2008; Yasarawan *et al*., 2014). Pople's split-valence triple-zeta basis set such as 6–311++G(d,p) was adopted to all computations. For such a basis set, the core orbital is described by a contracted set of six primitive Gaussians, and the valence orbital by a contracted set of three primitive Gaussians and two other sets of one Gaussian. The notation ++ indicates that a set of diffuse functions are included to heavy atoms and hydrogen. The notation (d,p) denotes the inclusion of d-polarization functions to non-hydrogen atoms and p-polarization functions to hydrogen. In the previous work, the 6–311++G(d,p) basis set has been used in describing the IPT reactions of various hydroxycoumarins (Yasarawan *et al*., 2014). The optimized ground-state geometries were taken to the process of vibrational frequency calculations, where the zero-point corrected electronic energies and thermodynamic parameters were evaluated. Solvation effect was taken into account by repeating the geometry optimizations with the application of polarizable continuum model (PCM) of solvation. In the PCM methodology, the solute molecule was placed in a theoretical cavity surrounded by a polarizable dielectric continuum of water (dielectric constant = 78.39). The non-electrostatic terms and atomic radii for such a solvation cavity were defined based on the solute electron density (Marenich *et al*., 2009).The transition-state (TS) geometry formed upon each reaction of interest was determined using the synchronous transit-guided quasi-Newton approach with the QST2 mode of calculation. The presence of a single imaginary vibrational frequency was used as an indication of the optimized geometry being a transition state. The activation energy ($\Delta E^{\ddagger}$) was determined from the energy of the transition-state structure minus that of the reactant structure. The rate constant (k) of each reaction at a given temperature T can be determined using the equation (Laidler & King, 1983):

$$k = \kappa \cdot \frac{k_B T}{h} \cdot \frac{Q^{TS}}{Q^{R}} \cdot \exp(-\Delta E^{\ddagger}/RT), \quad (1)$$

where k_B is the Boltzmann constant, *h* the Planck constant and *R* the gas constant. Q^{TS} and Q^{R} denote the total partition functions of the transition-state and reactant geometries, respectively. The Wigner transmission coefficient, κ, which accounts for the barrier-tunneling correction, is calculated as (Hirschfelder & Wigner, 1939):

$$\kappa = 1 + \frac{1}{24}\left(\frac{h\nu_i}{k_B T}\right)^2, \quad (2)$$

where ν_i is the imaginary vibrational frequency of the transition-state geometry. Eq (2) was formerly used in determining rate constants of IPT in various organic compounds (Suwattanamala & Ruangpornvisuti, 2009; Yasarawan *et al*., 2014).

Results and Discussion

Structural stability and intramolecular hydrogen bonding

The IPT and rotamerization reaction paths for all kaempferol-based compounds tested are shown in Figure 1 - 4. The transfer of H3 from the oxygen atom in the hydroxyl group at C3 to the vicinal carbonyl oxygen atom (O4) converts the normal form of each compound (denoted by the code "N") into the zwitterionic form (denoted by the code "Z"). According to the geometry optimizations in solution, the transfer of either H5 from O5 to O4, or H2* from O2* to O1 is so unfavorable that the Z forms are eventually converged back to the respective N forms. Thus the further discussion will be dedicated to the IPT from O3 to O4. Based on the relative total energies, the thermodynamic stability of molecular structure decreases in the order: N1 > N2 > Z1 > Z2, implying the higher affinity of H3 to bind to O3 than to O4 in every compound attempted. Note that the suffixes "1" and "2" are used to differentiate between two rotamers. The rotation of ring B (planar ring) about the C2–C1* axis can bring the O2*–H2* group to the same side as O3 (rotamer 1) or O1 (rotamer 2), except for kaempferol whose ring B is symmetric to such a rotation. Potential energy surface (PES) scanning reveals that rotamer 1 is more stable than the respective rotamer 2. The PES scan plots for morin are shown as example in Figure 5, with the global and local minima corresponding to rotamer 1 and rotamer 2, respectively. The preferential orientation of ring B in each rotamer 1 is in excellent agreement with the crystallographic data of zinc-morin complexes (Pieniazek *et al*., 2014). The vibrational frequency at 1200 cm^{-1} for the asymmetric S–O stretching in the N1 form of morin-5*-sulfonate (N5*SOM1) determined at the CAM-B3LYP/6-311++G(d,p) level is close to the experimental value at 1197 cm^{-1} (Pieniazek *et al*., 2014).

As evident in all structures (Figure 1 - 4), H2* could presumably interact with either O3 (in rotamer 1) or with O1 (in rotamer 2) through hydrogen bonding. The selected O–H distances in various species of morin are displayed in Table 1. Based on such structural data of all studied compounds, O3···H2* in every rotamer 1 (1.4 - 1.6 Å) and O1···H2* in every rotamer 2 (c.a. 2 Å) are shorter than the sum of the van der Waals radii of H and O atoms (i.e. 2.7 Å) (Bondi, 1964) but significantly longer than the adjacent O2*–H2* covalent bonds (c.a. 1 Å). The O2*–H2*···O3 angles are c.a. 160° and 170° for the N1 and Z1 forms, respectively, whereas the O2*–H2*···O1 angles are much narrower at c.a. 140° for both N2 and Z2 forms. Following the characteristics of typical hydrogen bonds reported in the literature (Parthasarathi & Subramanian, 2006), either O3···H2* in rotamer 1's or O1···H2* in rotamer 2's can be the medium hydrogen bonding with primary electrostatic character.

Electrostatic force between a pair of X and Y atoms can be estimated with the Coulomb relation: $q_X q_Y / r^2_{X-Y}$, where $q_X q_Y$ and r_{X-Y} are the product of the charge values of both atoms and the X-Y interatomic distance, respectively. Such an electrostatic force between two hydrogen-bonded atoms can be used as a measure of the hydrogen bond strength. The electrostatic forces between O and H atoms in the forms of morin are presented in Table 2. Based on the calculations at CAM-B3LYP/6-311++G(d,p) level, the O3···H2* attractive force (e^2 Å^{-2}) in rotamer 1 has been found to increase in the following order: morin-5*-sulfonate (N5*SOM1, -0.1318) < morin (NM1, -0.1323) < morin-7-O-sulfate (N7SAM1, -0.1375) < morin-5*-sulfonate (Z5*SOM1, -0.1835) < morin (ZM1, -0.1850) < morin-7-O-sulfate (Z7SAM1, -0.1876). Interestingly, for either N1 or Z1 forms, the strongest reinforcement of O3···H2* is achievable through the presence of 7-O-sulfate group. Also, O3···H2* is stronger in the Z1 form than in the corresponding N1 form, primarily due to the higher negative charge on O3 in the former (see Table 3). In summary, for all rotamer 2's, the O1···H2* attractive forces (e^2 Å^{-2}) are in the following order: morin (Z2, -8.03×10^{-2}) < morin-5*-sulfonate (Z2, -8.22×10^{-2}) < morin-7-O-sulfate (Z2, -8.42×10^{-2}) < morin-5*-sulfonate (N2, -8.50×10^{-2}) < morin (N2, -8.56×10^{-2}) < morin-7-O-sulfate (N2, -9.02×10^{-2}). Thus, the addition of 7-O-sulfate group results in the strongest O1···H2* for rotamer 2's as well. For any compounds tested, the hydrogen bond O3···H2* in rotamer 1 is stronger than O1···H2* in rotamer 2, giving a satisfactory explanation for the superior stability of rotamer 1 to rotamer 2. The endothermic nature of rotamerization (see ΔH_r values in Table 4) suggests that the enthalpy absorbed in the dissociation of O3···H2* is greater than the enthalpy released though the formation of O1···H2*, lending support to the theory that O3···H2* is stronger than O1···H2*. The strength of O3···H2* in either N1 or Z1 is correlated to the rotamerization enthalpy in such a way that the stronger O3···H2* in rotamer 1 yields the higher rotamerization enthalpy. Compared to the N form, the rotamerization of the corresponding Z form is not as much favorable since the rotation of ring B in the Z form is more highly restricted by the stronger O3···H2*.

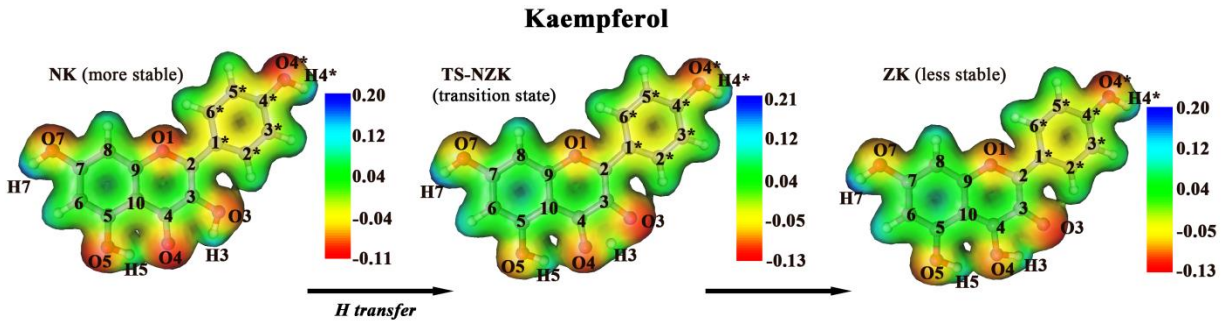

Figure 1 IPT and rotamerization paths for kaempferol. Electrostatic potential (ESP) maps were built with isosurface value of 0.010e Å^{-3}. All structures were optimized at PCM-DFT/CAM-B3LYP/6-311++G(d,p) level.

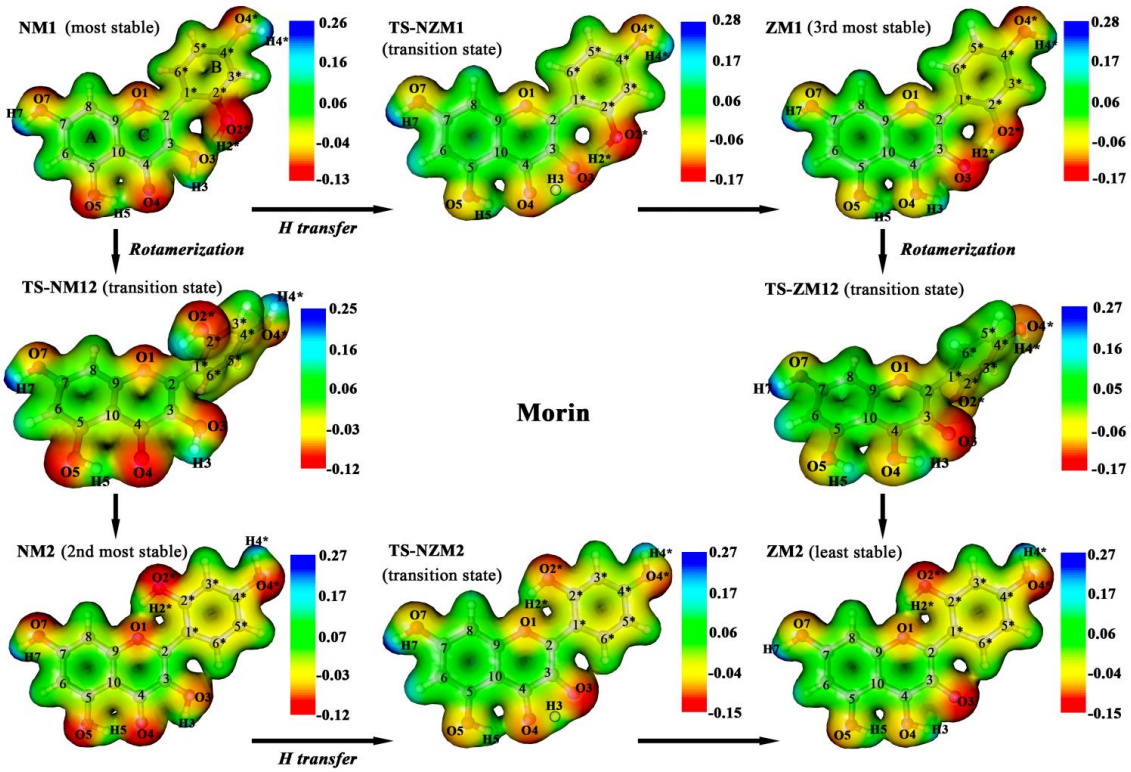

Figure 2 IPT and rotamerization paths for morin. Electrostatic potential (ESP) maps were built with isosurface value of 0.010e Å^{-3}. All structures were optimized at PCM-DFT/CAM-B3LYP/6-311++G(d,p) level.

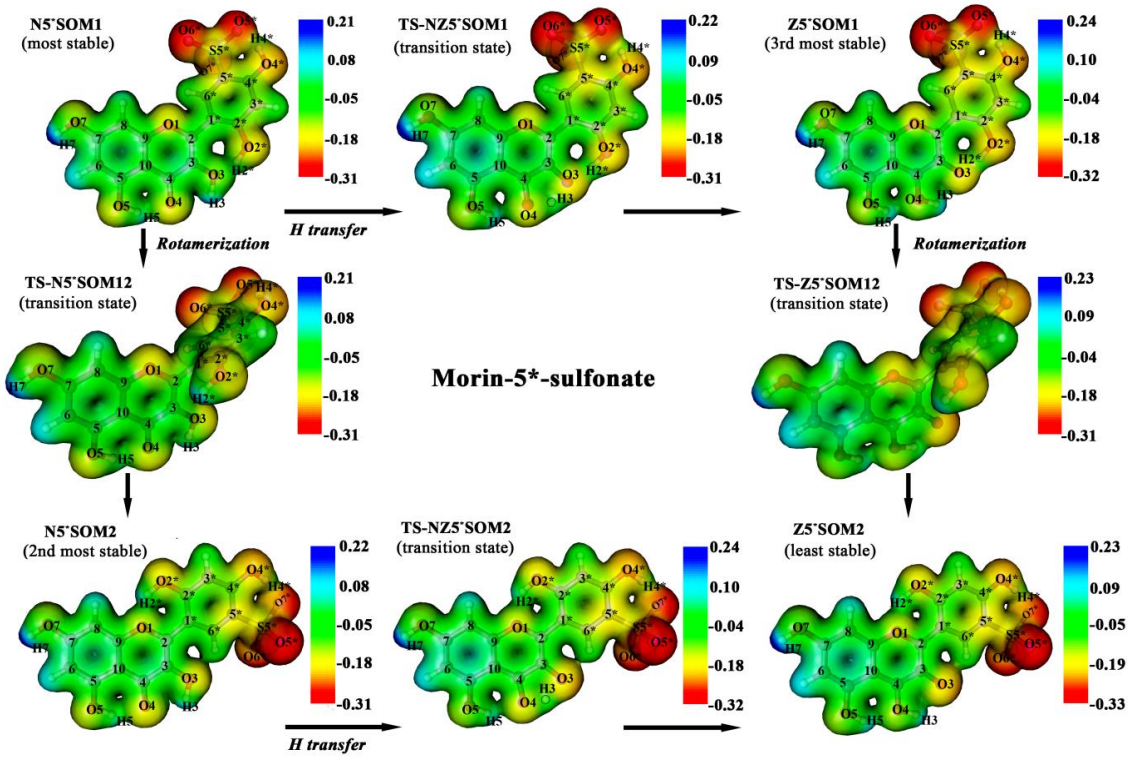

Figure 3 IPT and rotamerization paths for morin-5*-sulfonate. Electrostatic potential (ESP) maps were built with isosurface value of 0.010e Å^{-3}. All structures were optimized at PCM-DFT/CAM-B3LYP/6-311++G (d,p) level.

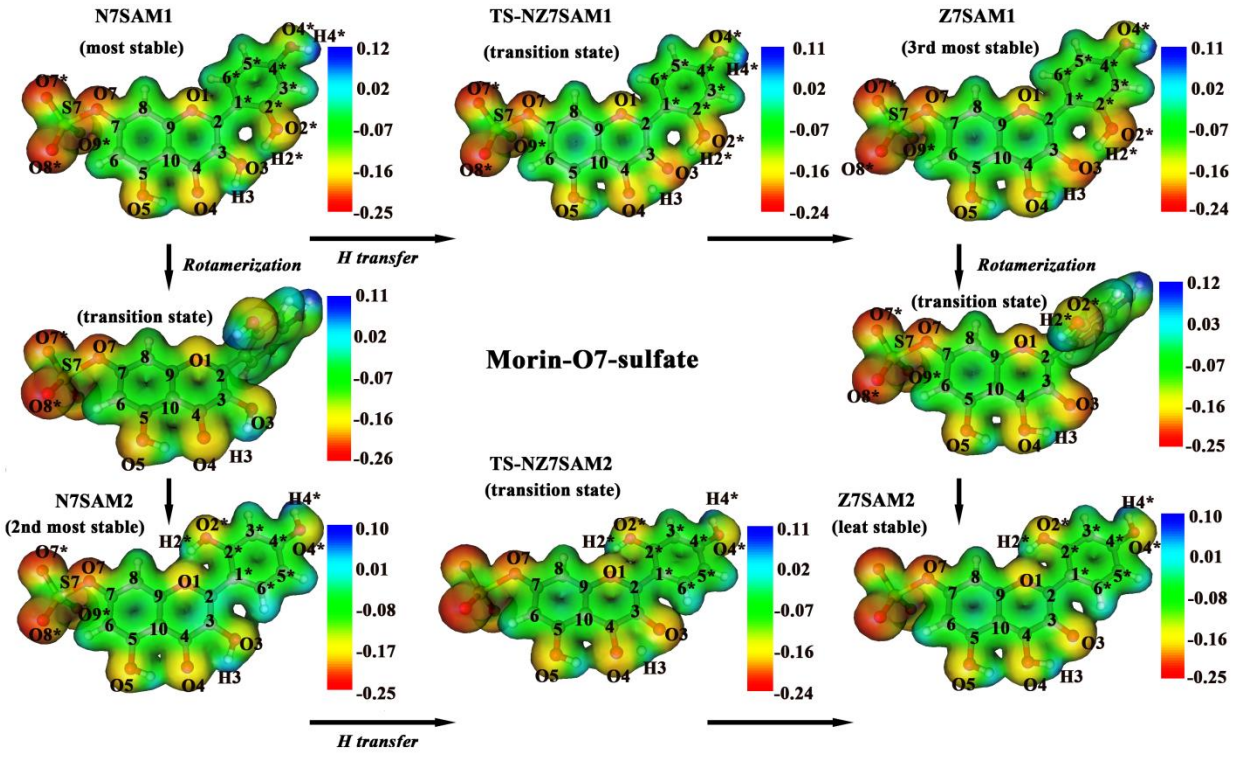

Figure 4 IPT and rotamerization paths for morin-7-O-sulfate. Electrostatic potential (ESP) maps were built with isosurface value of 0.010e Å^{-3}. All structures were optimized at PCM-DFT/CAM-B3LYP/6-311++G(d,p) level.

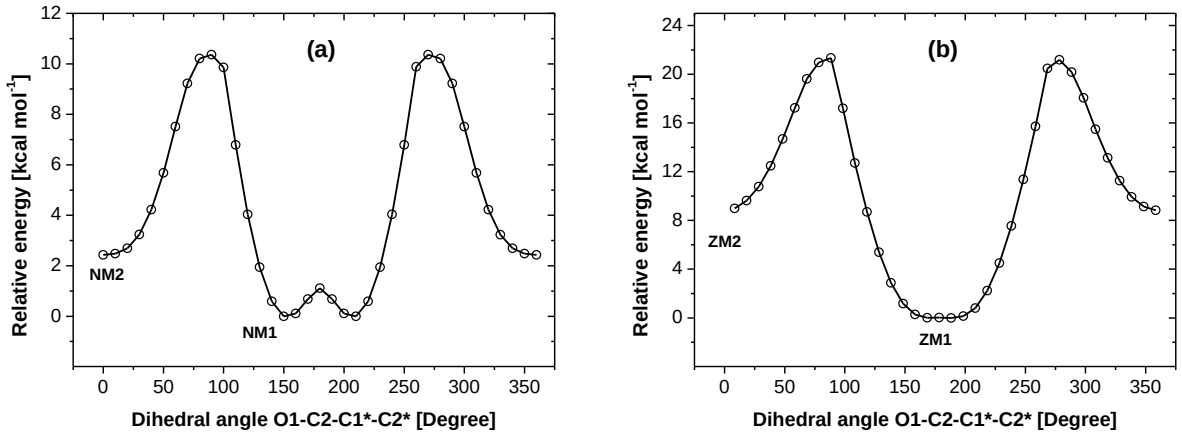

Figure 5 Potential energy surface scans of (a) normal form [NM] and (b) zwitterionic form [ZM] of morin based on the computations at PCM-DFT/CAM-B3LYP/6-311++G(d,p) level.

Table 1 Selected O-H interatomic distances (Å) for forms of morin including IPT transition states.

	O1-H2*	O3-H2* [(a)]	O3-H3 [(a)]	O4-H3 [(a)]	O4-H5 [(a)]	O5-H5 [(a)]	O7-H7 [(a)]	O2*-H2* [(a)]	O4*-H4* [(a)]
NM1	—	1.637 [1.630] [(b)]	0.985 [0.989]	2.047 [2.221] [(b)]	1.788 [1.773] [(b)]	0.995 [0.996]	0.972 [0.988]	0.989 [0.993]	0.972 [0.988]
ZM1	—	1.447 [1.431] [(b)]	1.896 [2.102] [(b)]	0.999 [0.994]	1.875 [1.860] [(b)]	0.981 [0.983]	0.972 [0.989]	1.041 [1.050]	0.972 [0.988]
TS-NZM1	—	1.540 [1.548] [(b)]	1.343 [1.328]	1.206 [1.223]	1.929 [1.977] [(b)]	0.985 [0.984]	0.972 [0.989]	1.012 [1.011]	0.972 [0.988]
NM2	1.751 [1.747] [(b)]	—	0.985 [0.989]	2.037 [2.133] [(b)]	1.771 [1.767] [(b)]	0.996 [0.996]	0.972 [0.989]	0.977 [0.978]	0.972 [0.988]
ZM2	1.777 [1.772] [(b)]	—	1.846 [2.024] [(b)]	1.010 [1.000]	1.868 [1.857] [(b)]	0.982 [0.983]	0.972 [0.989]	0.976 [0.978]	0.972 [0.988]
TS-NZM2	1.786 [1.785] [(b)]	—	1.422 [1.394]	1.160 [1.177]	1.911 [1.951] [(b)]	0.985 [0.985]	0.972 [0.989]	0.976 [0.978]	0.972 [0.988]

[(a)] Numbers inside and outside of square brackets belong to the hydrated geometries optimized at B3LYP/ 6-311++G(d,p) and CAM-B3LYP/6-311++G(d,p) levels, respectively.

[(b)] Intramolecular hydrogen bond.

Table 2 Electrostatic forces (e^2 $Å^{-2}$) between selected O and H atoms estimated with the Coulomb relation for various species of morin.

	O1-H2*	O3-H2* [(a)]	O3-H3 [(a)]	O4-H3 [(a)]	O4-H5 [(a)]	O5-H5 [(a)]	O7-H7 [(a)]	O2*-H2* [(a)]	O4*-H4* [(a)]
NM1	-	-0.132 [-0.136] [(b)]	-0.374 [-0.399]	-0.083 [-0.077] [(b)]	-0.108 [-0.113] [(b)]	-0.337 [-0.350]	-0.326 [-0.368]	-0.353 [-0.365]	-0.326 [-0.369]
ZM1	-	-0.185 [-0.192] [(b)]	-0.113 [-0.099] [(b)]	-0.357 [-0.374]	-0.099 [-0.102] [(b)]	-0.349 [-0.364]	-0.325 [-0.366]	-0.307 [-0.317]	-0.326 [-0.368]
NM2	-0.086 [-0.086] [(b)]	-	-0.347 [-0.370]	-0.081 [-0.080] [(b)]	-0.109 [-0.114] [(b)]	-0.336 [-0.350]	-0.327 [-0.367]	-0.350 [-0.365]	-0.325 [-0.369]
ZM2	-0.080 [-0.081] [(b)]	-	-0.113 [-0.105] [(b)]	-0.345 [-0.365]	-0.099 [-0.102] [(b)]	-0.348 [-0.364]	-0.326 [-0.366]	-0.348 [-0.363]	-0.324 [-0.367]

[(a)] Numbers inside and outside of square brackets belong to the hydrated geometries optimized at B3LYP/ 6-311++G(d,p) and CAM-B3LYP/6-311++G(d,p) levels, respectively.

[(b)] Intramolecular hydrogen bond.

Table 3 Natural atomic charges (q) and electronic populations (pop) in kaempferol-based compounds determined at CAM-B3LYP/6-311++G(d,p) level of theory.

NK			ZK			NM1			ZM1		
Atom	q [e]	pop	Atom	q [e]	pop	Atom	q [e]	pop	Atom	q [e]	pop
C1*	-0.130	6.130	C1*	-0.135	6.135	C1*	-0.199	6.199	C1*	-0.207	6.207
C6*	-0.148	6.148	C6*	-0.148	6.148	C6*	-0.131	6.131	C6*	0.400	5.600
C5*	-0.243	6.243	C5*	-0.245	6.245	C5*	-0.268	6.268	C5*	-0.337	6.337
C4*	0.334	5.666	C4*	0.337	5.663	C4*	0.351	5.649	C4*	0.359	5.641
C3*	-0.282	6.282	C3*	-0.284	6.284	C3*	-0.327	6.327	C3*	-0.271	6.271
C2*	-0.147	6.147	C2*	-0.141	6.141	C2*	0.377	5.623	C2*	-0.133	6.133
C6	-0.343	6.343	C7	-0.337	6.337	C6	-0.341	6.341	C6	-0.333	6.333
C7	0.366	5.634	C8	0.360	5.640	C7	0.368	5.632	C7	0.361	5.639
C8	-0.316	6.316	C5	-0.311	6.311	C8	-0.313	6.313	C8	-0.309	6.309
C5	0.395	5.605	C10	0.384	5.616	C5	0.395	5.605	C5	0.381	5.619
C10	-0.250	6.250	C9	-0.234	6.234	C10	-0.249	6.249	C10	-0.229	6.229
C9	0.374	5.626	O1	0.377	5.623	C9	0.373	5.627	C9	0.375	5.625
O1	-0.488	8.488	C2	-0.468	8.468	O1	-0.485	8.485	O1	-0.474	8.474
C2	0.331	5.669	C3	0.331	5.669	C2	0.342	5.658	C2	0.356	5.644
C3	0.201	5.799	C4	0.234	5.766	C3	0.181	5.819	C3	0.219	5.781
C4	0.414	5.586	C4	0.378	5.622	C4	0.415	5.585	C4	0.372	5.628
O4	-0.685	8.685	O4	-0.687	8.687	O4	-0.687	8.687	O4	-0.786	8.786
H6*	0.226	0.774	H6*	0.221	0.779	H6*	0.224	0.776	H6*	-0.688	8.688
H5*	0.225	0.775	H5*	0.224	0.776	H5*	0.226	0.774	H5*	0.225	0.775
H3*	0.206	0.794	H3*	0.207	0.793	H6	0.229	0.772	H6	0.225	0.775
H2*	0.245	0.755	H2*	0.258	0.742	H8	0.246	0.754	H8	0.230	0.770
H6	0.227	0.773	H6	0.229	0.771	O5	-0.665	8.665	O5	0.247	0.753
H8	0.244	0.756	H8	0.246	0.754	H5	0.501	0.499	H5	-0.666	8.666
O5	-0.667	8.667	O5	-0.666	8.666	O7	-0.658	8.658	O7	-0.657	8.657
H5	0.501	0.499	H5	0.504	0.496	H7	0.468	0.532	H7	0.518	0.482
O7	-0.660	8.660	O7	-0.657	8.657	O3	-0.712	8.712	O3	0.468	0.532
H7	0.467	0.533	H7	0.468	0.532	H3	0.509	0.491	H3	-0.660	8.660
O3	-0.684	8.684	O3	-0.751	8.751	O4*	-0.663	8.663	O4*	0.224	0.776
H3	0.492	0.508	H3	0.510	0.490	H4*	0.464	0.536	H4*	-0.675	8.675
O4*	-0.666	8.666	O4*	-0.665	8.665	H3*	0.225	0.775	H3*	0.493	0.507
H4*	0.463	0.537	H4*	0.463	0.537	O2*	-0.693	8.693	O2*	0.466	0.534
						H2*	0.498	0.502	H2*	0.504	0.496

Table 3 (continued) Natural atomic charges (q) and electronic populations (pop) in kaempferol-based compounds determined at CAM-B3LYP/6-311++G(d,p) level of theory.

N5*SOM1			Z5*SOM1			N7SAM1			Z7SAM1		
Atom	q [e]	pop	Atom	q [e]	pop	Atom	q [e]	pop	Atom	q [e]	pop
C1*	-0.210	6.210	C1*	-0.205	6.205	C1*	-0.186	6.186	C1*	-0.196	6.196
C6*	-0.141	6.141	C6*	-0.142	6.142	C6*	-0.133	6.133	C6*	-0.138	6.138
C5*	-0.240	6.240	C5*	-0.236	6.236	C5*	-0.276	6.276	C5*	-0.284	6.284
C4*	0.358	5.642	C4*	0.369	5.631	C4*	0.337	5.663	C4*	0.339	5.661
C3*	-0.296	6.296	C3*	-0.309	6.309	C3*	-0.332	6.332	C3*	-0.340	6.340
C2*	0.371	5.629	C2*	0.395	5.605	C2*	0.368	5.632	C2*	0.383	5.617
C6	-0.350	6.350	C6	-0.341	6.341	C6	-0.319	6.319	C6	-0.310	6.310
C7	0.359	5.641	C7	0.347	5.653	C7	0.389	5.611	C7	0.392	5.608
C8	-0.310	6.310	C8	-0.303	6.303	C8	-0.314	6.314	C8	-0.314	6.314
C5	0.388	5.612	C5	0.370	5.630	C5	0.381	5.619	C5	0.368	5.632
C10	-0.247	6.247	C10	-0.228	6.228	C10	-0.256	6.256	C10	-0.232	6.232
C9	0.375	5.625	C9	0.372	5.628	C9	0.357	5.643	C9	0.368	5.632
O1	-0.478	8.478	O1	-0.474	8.474	O1	-0.495	8.495	O1	-0.482	8.482
C2	0.357	5.643	C2	0.368	5.632	C2	0.320	5.680	C2	0.323	5.677
C3	0.167	5.833	C3	0.219	5.781	C3	0.184	5.816	C3	0.210	5.790
C4	0.403	5.597	C4	0.339	5.661	C4	0.406	5.594	C4	0.385	5.615
O4	-0.714	8.714	O4	-0.709	8.709	O4	-0.713	8.713	O4	-0.692	8.692
H6*	0.251	0.749	H6*	0.253	0.747	H6*	0.228	0.772	H6*	0.225	0.775
H6	0.220	0.780	H6	0.220	0.780	H5*	0.220	0.780	H5*	0.218	0.782
H8	0.254	0.746	H8	0.255	0.745	H6	0.263	0.737	H6	0.265	0.735
O5	-0.679	8.679	O5	-0.682	8.682	H8	0.236	0.764	H8	0.238	0.762
H5	0.498	0.502	H5	0.501	0.499	O5	-0.676	8.676	O5	-0.673	8.673
O7	-0.662	8.662	O7	-0.663	8.663	H5	0.491	0.509	H5	0.492	0.508
H7	0.460	0.540	H7	0.459	0.541	O7	-0.651	8.651	O7	-0.644	8.644
O3	-0.716	8.716	O3	-0.796	8.796	O3	-0.724	8.724	O3	-0.807	8.807
H3	0.503	0.497	H3	0.512	0.488	H3	0.506	0.494	H3	0.511	0.489
O4*	-0.669	8.669	O4*	-0.659	8.659	O4*	-0.676	8.676	O4*	-0.677	8.677
H4*	0.496	0.504	H4*	0.495	0.505	H4*	0.457	0.543	H4*	0.456	0.544
H3*	0.233	0.767	H3*	0.234	0.766	H3*	0.217	0.783	H3*	0.215	0.785
O2*	-0.701	8.701	O2*	-0.681	8.681	O2*	-0.703	8.703	O2*	-0.700	8.700
H2*	0.493	0.507	H2*	0.490	0.510	H2*	0.499	0.501	H2*	0.492	0.508
S5*	1.809	14.191	S5*	1.809	14.191	S7	1.898	14.102	S7	1.894	14.106
O7*	-0.835	8.835	O7*	-0.832	8.832	O7*	-0.754	8.754	O7*	-0.746	8.746
O6*	-0.844	8.844	O6*	-0.842	8.842	O8*	-0.784	8.784	O8*	-0.779	8.779
O5*	-0.905	8.905	O5*	-0.903	8.903	O9*	-0.765	8.765	O9*	-0.760	8.760

Table 3 (continued) Natural atomic charges (q) and electronic populations (pop) in kaempferol-based compounds determined at CAM-B3LYP/6-311++G(d,p) level of theory.

NM2			ZM2			N5*SOM2			Z5*SOM2		
Atom	q [e]	pop	Atom	q [e]	pop	Atom	q [e]	pop	Atom	q [e]	pop
C1*	-0.201	6.20	C1*	-0.199	6.20	C1*	-0.210	6.21	C1*	-0.201	6.20
C6*	-0.136	6.14	C6*	0.374	5.63	C6*	-0.146	6.15	C6*	-0.140	6.14
C5*	-0.269	6.27	C5*	-0.335	6.34	C5*	-0.241	6.24	C5*	-0.242	6.24
C4*	0.353	5.65	C4*	0.357	5.64	C4*	0.360	5.64	C4*	0.370	5.63
C3*	-0.332	6.33	C3*	-0.270	6.27	C3*	-0.299	6.30	C3*	-0.302	6.30
C2*	0.372	5.63	C2*	-0.131	6.13	C2*	0.366	5.63	C2*	0.369	5.63
C6	-0.340	6.34	C6	-0.334	6.33	C6	-0.350	6.35	C6	-0.343	6.34
C7	0.368	5.63	C7	0.362	5.64	C7	0.357	5.64	C7	0.342	5.66
C8	-0.320	6.32	C8	-0.316	6.32	C8	-0.323	6.32	C8	-0.318	6.32
C5	0.397	5.60	C5	0.386	5.61	C5	0.391	5.61	C5	0.375	5.63
C10	-0.248	6.25	C10	-0.232	6.23	C10	-0.243	6.24	C10	-0.229	6.23
C9	0.373	5.63	C9	0.375	5.63	C9	0.373	5.63	C9	0.366	5.63
O1	-0.531	8.53	O1	-0.515	8.51	O1	-0.532	8.53	O1	-0.521	8.52
C2	0.335	5.67	C2	0.334	5.67	C2	0.348	5.65	C2	0.350	5.65
C3	0.198	5.80	C3	0.233	5.77	C3	0.189	5.81	C3	0.237	5.76
C4	0.413	5.59	C4	0.373	5.63	C4	0.399	5.60	C4	0.333	5.67
O4	-0.683	8.68	O4	-0.749	8.75	O4	-0.702	8.70	O4	-0.708	8.71
H6*	0.248	0.75	H6*	-0.687	8.69	H6*	0.273	0.73	H6*	0.285	0.72
H5*	0.226	0.77	H5*	0.225	0.78	H6	0.221	0.78	H6	0.221	0.78
H6	0.229	0.77	H6	0.227	0.77	H8	0.239	0.76	H8	0.239	0.76
H8	0.243	0.76	H8	0.230	0.77	O5	-0.677	8.68	O5	-0.679	8.68
O5	-0.664	8.66	O5	0.244	0.76	H5	0.500	0.50	H5	0.504	0.50
H5	0.502	0.50	H5	-0.664	8.66	O7	-0.668	8.67	O7	-0.670	8.67
O7	-0.658	8.66	O7	-0.657	8.66	H7	0.461	0.54	H7	0.460	0.54
H7	0.469	0.53	H7	0.512	0.49	O3	-0.670	8.67	O3	-0.733	8.73
O3	-0.682	8.68	O3	0.469	0.53	H3	0.491	0.51	H3	0.510	0.49
H3	0.494	0.51	H3	-0.659	8.66	O4*	-0.667	8.67	O4*	-0.657	8.66
O4*	-0.662	8.66	O4*	0.261	0.74	H4*	0.494	0.51	H4*	0.490	0.51
H4*	0.464	0.54	H4*	-0.674	8.67	H3*	0.233	0.77	H3*	0.234	0.77
H3*	0.225	0.77	H3*	0.492	0.51	O2*	-0.685	8.69	O2*	-0.681	8.68
O2*	-0.677	8.68	O2*	0.464	0.54	H2*	0.487	0.51	H2*	0.487	0.51
H2*	0.494	0.51	H2*	0.505	0.50	S7	1.810	14.19	S7	1.810	14.19
						O5*	-0.833	8.83	O5*	-0.829	8.83
						O6*	-0.839	8.84	O6*	-0.827	8.83
						O7*	-0.906	8.91	O7*	-0.903	8.90

Table 3 (continued) Natural atomic charges (q) and electronic populations (pop) in kaempferol-based compounds determined at CAM-B3LYP/6-311++G(d,p) level of theory.

N7SAM2			Z7SAM2		
Atom	q [e]	pop	Atom	q [e]	pop
C1*	-0.189	6.19	C1*	-0.188	6.19
C6*	-0.144	6.14	C6*	-0.144	6.14
C5*	-0.279	6.28	C5*	-0.280	6.28
C4*	0.337	5.66	C4*	0.335	5.66
C3*	-0.335	6.33	C3*	-0.339	6.34
C2*	0.366	5.63	C2*	0.363	5.64
C6	-0.320	6.32	C6	-0.312	6.31
C7	0.390	5.61	C7	0.393	5.61
C8	-0.321	6.32	C8	-0.321	6.32
C5	0.384	5.62	C5	0.372	5.63
C10	-0.258	6.26	C10	-0.237	6.24
C9	0.358	5.64	C9	0.369	5.63
O1	-0.541	8.54	O1	-0.526	8.53
C2	0.312	5.69	C2	0.297	5.70
C3	0.202	5.80	C3	0.227	5.77
C4	0.407	5.59	C4	0.384	5.62
O4	-0.707	8.71	O4	-0.693	8.69
H6*	0.245	0.75	H6*	0.257	0.74
H5*	0.218	0.78	H5*	0.217	0.78
H6	0.264	0.74	H6	0.266	0.73
H8	0.232	0.77	H8	0.235	0.77
O5	-0.675	8.67	O5	-0.672	8.67
H5	0.492	0.51	H5	0.493	0.51
O7	-0.652	8.65	O7	-0.645	8.65
O3	-0.694	8.69	O3	-0.772	8.77
H3	0.489	0.51	H3	0.503	0.50
O4*	-0.676	8.68	O4*	-0.677	8.68
H4*	0.457	0.54	H4*	0.455	0.54
H3*	0.219	0.78	H3*	0.217	0.78
O2*	-0.683	8.68	O2*	-0.685	8.69
H2*	0.500	0.50	H2*	0.496	0.50
S7	1.898	14.10	S7	1.893	14.11
O7*	-0.753	8.75	O7*	-0.745	8.74
O8*	-0.782	8.78	O8*	-0.778	8.78
O9*	-0.763	8.76	O9*	-0.758	8.76

Thermodynamics of IPT reactions

The essential thermodynamic parameters for the IPT reactions taking place in all kaempferol-based compounds are summarized in Table 4. Compared to the rotamerization, the IPT is not as much favorable. This is reasonable as each IPT is associated with either bond dissociation or bond formation. The IPT reactions in aqueous phase at the standard state of 1 M and 298 K are endothermic (positive enthalpy change) and non-spontaneous (positive Gibbs energy). The entropy changes are so negligible that the spontaneity of reaction is dictated by the enthalpy changes. Based on the IPT Gibbs energies (ΔG_r), the IPT potential of the N1 form increases in the following sequence: morin < morin-5*-sulfonate < morin-7-O-sulfate. The IPT potential of the N2 form also increases in the same sequence. In reference to kaempferol (ΔG_r = 15.8 kcal mol^{-1}), the IPT potential can be therefore promoted by any substituents tested and the strongest enhancement of the IPT potential is obtained by the co-addition of O2*–H2* and 7-O-sulfate groups to the parent kaempferol skeleton. Furthermore, the IPT in the N1 form is much more favorable than that in the respective N2 form. Basically, the potential for each compound to undergo the IPT reaction depends on how well the substituent can deal with the electronic instability caused by the charge polarization within each zwitterionic structure. As seen in the electrostatic potential (ESP) maps in Figure 1, the Z form of kaempferol (ZK) displays peculiarly high negative charge populations over O3 and ring B, implying marked electronic instability. On the other hand, the additional O2*–H2* group in the Z1 of morin (ZM1 in Figure 2) renders the negative charge distribution on the three-ring skeleton more homogeneous, hence highly promoting electronic stability. Clearly, the negative charges over the entire three-ring skeleton are distributed most uniformly in the Z1 form of morin-7-O-sulfate (Z7SAM1 in Figure 4) compared to the Z1 forms of the other compounds, hence corresponding well to the highest IPT potential of morin-7-O-sulfate.

Kinetics of IPT reactions

Essential kinetic parameters for the IPT reactions at 298 K in aqueous phase are summarized in Table 5. Based on the rate constants (*k*), the IPT of each N1 form is found to be extremely faster than that of the respective N2 form. The energy profiles for the IPT for both NM1 and NM2 of morin are shown in Figure 6 as example. No signs of intermediates are observed along the reaction coordinate. So far, the IPT of N1 is more favorable than that of its rotamer (N2), not only thermodynamically but also kinetically. Regarding the N1 forms, any chemical substituents attempted in this work can highly accelerate the IPT relative to parent kaempferol structure. The IPT rate constant for the N1 form in aqueous solution increases in the sequence: morin < morin-5*-sulfonate < morin-7-O-sulfate. The same sequence is applicable to the rate constants for the N2 forms. Interestingly, the most enhanced IPT kinetics of morin-7-O-sulfate coincides with its strongest thermodynamic IPT potential. The IPT activation energy ($\Delta E^{\ddagger}$) is decreased from the reference value of kaempferol by as much as 30%, 40% and 45% for the N1 forms of morin, morin-5*-sulfonate and morin-7-O-sulfate, respectively; hence the enhanced IPT kinetics is mainly attributed to the decrease in activation energy.

Table 4 Thermodynamic parameters for intramolecular proton transfer (IPT) and rotamerization (Rot) in aqueous solution of various kaempferol-based species determined at two levels of theory.

	Reaction	Type	PCM-DFT/B3LYP/6-311++G(d,p) Level				PCM-DFT/CAM-B3LYP/6-311++G(d,p) Level			
			$\Delta E_r^{(a,b)}$	$\Delta H_r^{(a,b)}$	$\Delta S_r^{(a,b)}$	$\Delta G_r^{(a,b)}$	$\Delta E_r^{(a,b)}$	$\Delta H_r^{(a,b)}$	$\Delta S_r^{(a,b)}$	$\Delta G_r^{(a,b)}$
Kaempferol	NK → ZK	IPT	15.7	15.7	-0.34	15.8	15.3	15.3	-0.32	15.4
Morin	NM1 → ZM1	IPT	8.57 (6.17)	11.4 (8.3)	1.01 (0.34)	11.1 (9.0)	8.38 (6.03)	11.1 (8.11)	0.99 (0.33)	10.9 (8.79)
	NM2 → ZM2	IPT	18.6 (16.2)	19.2 (16.1)	6.04 (5.37)	17.4 (15.3)	18.2 (15.8)	18.8 (15.7)	5.91 (5.25)	17.0 (14.9)
	NM1 → NM2	Rot	2.40 (0)	3.10 (0)	3.32 (2.65)	2.11 (0)	2.35 (0)	3.03 (0)	3.25 (2.59)	2.06 (0)
	ZM1 → ZM2	Rot	10.1 (7.7)	9.60 (6.5)	0.67 (0)	9.40 (7.29)	9.87 (7.53)	9.39 (6.36)	0.66 (0)	9.19 (7.13)
Morin-5*-sulfonate	N5*SOM1 → Z5*SOM1	IPT	8.30 (5.13)	8.38 (5.06)	2.25 (2.92)	7.71 (5.09)	8.09 (5.00)	8.13 (4.91)	2.19 (2.85)	7.52 (4.96)
	N5*SOM2 → Z5*SOM2	IPT	16.7 (13.5)	16.8 (13.5)	-0.34 (0.34)	16.9 (14.3)	16.3 (13.2)	16.3 (13.1)	-0.33 (0.32)	16.5 (13.9)
	N5*SOM1 → N5*SOM2	Rot	3.17 (0)	3.32 (0)	2.35 (3.02)	2.62 (0)	3.09 (0)	3.22 (0)	2.29 (2.94)	2.55 (0)
	Z5*SOM1 → Z5*SOM2	Rot	11.6 (8.43)	11.7 (8.38)	-0.67 (0)	11.9 (9.28)	11.3 (8.22)	11.3 (8.13)	-0.65 (0)	11.6 (9.05)
Morin-7-O-sulfate	N7SAM1 → Z7SAM1	IPT	5.46 (3.84)	5.49 (3.73)	0.30 (1.98)	5.40 (4.66)	5.29 (3.72)	5.32 (3.61)	0.29 (1.92)	5.23 (4.52)
	N7SAM2 → Z7SAM2	IPT	12.6 (11.0)	12.7 (10.9)	-1.68 (0)	13.2 (12.5)	12.2 (10.6)	12.3 (10.6)	-1.63 (0)	12.8 (12.1)
	N7SAM1 → N7SAM2	Rot	1.62 (0)	1.76 (0)	3.42 (5.10)	0.74 (0)	1.57 (0)	1.71 (0)	3.31 (4.94)	0.72 (0)
	Z7SAM1 → Z7SAM2	Rot	8.76 (7.14)	8.93 (7.17)	1.28 (2.95)	8.55 (7.81)	8.49 (6.92)	8.65 (6.95)	1.24 (2.87)	8.28 (7.57)

[(a)] All numbers in parentheses are the values relative to the minimum for a given compound.

[(b)] ΔE_r = total energy change (kcal mol^{-1}), ΔH_r = enthalpy change (kcal mol^{-1}), ΔG_r = Gibbs energy change (kcal mol^{-1}) and ΔS_r = entropy change (cal mol^{-1}).

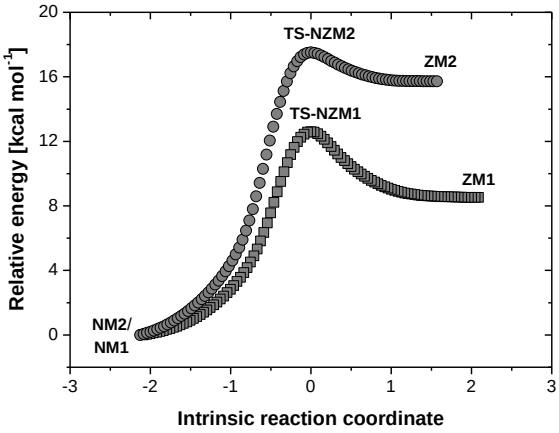

Figure 6 IPT reaction energy profiles for the IPT reactions in water of normal form (NM1) and zwitterionic form (ZM1) of morin. All data are based on the computations at PCM-DFT/CAM-B3LYP/6-311++G(d,p) level.

Let us consider the charge distribution over the TS geometries formed upon the IPT of all N1 forms. In the TS geometry of morin-7-O-sulfate (TS-NZ7SAM1 in Figure 4), the presence of 7-O-sulfate induces the displacement of more electrons from ring B to the chromone moiety, yielding a strikingly uniform distribution of negative charge density throughout the three-ring core structure. As the TS geometry for morin-7-O-sulfate has been electronically stabilized, the activation energy is expected to be low. The highest activation energy for kaempferol is consistent with the finding that the negative charges in its TS geometry (TS-NZK in Figure 1) are localized much more heavily on ring B than the other two rings. In the TS geometry of morin (TS-NZM1 in Figure 2), the additional $O2^{*}$–$H2^{*}$ permits the formation of $O3^{*}\cdots H2^{*}$ that favorably distributes the non-bonding electrons from O3 to the neighboring $O2^{*}$–$H2^{*}$. A significant portion of electrons are then allocated from the electron-rich moiety (i.e. ring B) to the chromone moiety, resulting in the more homogeneous electron density across the three-ring skeleton. Compared to the TS geometry of morin-7-O-sulfate mentioned above, the inductive effect due to $O3^{*}\cdots H2^{*}$ in the TS geometry of morin is not as much effective in homogenizing the charge density. This is because, at the same time, the $O2^{*}$–$H2^{*}$ group also increases the number of electrons on ring B. This observation agrees with the finding that the IPT activation energy is higher for morin than for morin-7-O-sulfate. For the TS geometry of morin-5^{*}-sulfonate (TS-NZ5^{*}SOM1 in Figure 3), because of the marked electron-withdrawing ability of the $C5^{*}$-sulfonate, the electron density over ring B is slightly higher than that over either ring A or ring C. This may explain why the IPT activation energy for morin-5^{*}-sulfonate is higher than that for morin-7-O-sulfate.

Table 5 Kinetic parameters for intramolecular hydrogen transfer (IPT) and rotamerization (Rot) in aqueous solution of various kaempferol-based species determined at PCM-DFT/CAM-B3LYP/6-311++G(d,p) level.

		Type	ν_i [(a)]	κ [(b)]	A [(c)]	$\Delta E^{\ddagger}$ [(d)]	k [(e)]
Kaempferol	NK ⟶ ZK	IPT	1102.8	2.18	8.95×10^{12}	17.7	0.950
Morin	NM1 ⟶ ZM1	IPT	1317.7	2.69	2.61×10^{13}	12.6 (2.8)	1.51×10^{4}
	NM2 ⟶ ZM2	IPT	1110.0	2.20	5.52×10^{12}	17.5 (7.7)	0.821
	NM1 ⟶ NM2	Rot	37.0	1.00	3.86×10^{12}	9.78 (0)	2.62×10^{5}
	ZM1 ⟶ ZM2	Rot	43.1	1.00	1.90×10^{12}	21.1 (11.3)	6.51×10^{-4}
Morin-5*-sulfonate	N5*SOM1 ⟶ Z5*SOM1	IPT	1327.5	2.71	3.98×10^{13}	10.5 (0)	8.31×10^{5}
	N5*SOM2 ⟶ Z5*SOM2	IPT	1127.7	2.24	6.74×10^{12}	16.5 (6.05)	5.42
	N5*SOM1 ⟶ N5*SOM2	Rot	28.6	1.00	2.80×10^{12}	11.8 (1.29)	6.61×10^{3}
	Z5*SOM1 ⟶ Z5*SOM2	Rot	35.8	1.00	1.36×10^{12}	24.9 (14.4)	7.73×10^{-7}
Morin-7-O-sulfate	N7SAM1 ⟶ Z7SAM1	IPT	1289.3	2.61	1.57×10^{13}	9.80 (0.08)	1.03×10^{6}
	N7SAM2 ⟶ Z7SAM2	IPT	1059.8	2.09	3.90×10^{12}	14.6 (4.88)	77.5
	N7SAM1 ⟶ N7SAM2	Rot	38.5	1.00	3.29×10^{12}	9.72 (0)	2.47×10^{5}
	Z7SAM1 ⟶ Z7SAM2	Rot	39.9	1.00	3.32×10^{12}	19.9 (10.2)	8.60×10^{-3}

[(a)] Imaginary part of transition-state vibrational frequency (cm^{-1}).

[(b)] Transmission coefficient.

[(c)] Arrhenius pre-exponential factor (s^{-1}).

[(d)] Activation energy (kcal mol^{-1}).

[(e)] Rate constant (s^{-1}).

Conclusions

In this study, both the conformational stability and intramolecular proton transfer reactions of four flavonols, namely kaempferol, morin, morin-5*-sulfonate and morin-7-O-sulfate in aqueous solution were investigated using the DFT/PCM approach, with the basis set 6-311++G(d,p) and the density functionals B3LYP and CAM-B3LYP. It has been found that for all of these flavonols, the formation of normal forms is more favorable than that of zwitterionic forms. The most stable conformation of each normal form requires the intramolecular hydrogen bonding between the hydrogen atom in the hydroxyl group at C2* and the oxygen atom in the hydroxyl group at position C3. In reference to the parent kaempferol molecule, the transfer of proton from the hydroxyl group at position C3 to the nearest carbonyl oxygen atom can be enhanced by any choices of substituents attempted in this work. On the basis of thermodynamics, the potential to undergo the intramolecular proton transfer decreases in the following order: morin-7-O-sulfate > morin-5*-sulfonate > morin > kaempferol. The same order also applies to the rate of proton transfer. The greatest potential to undergo such a proton transfer is achievable by the introduction of a sulfate group at position C7 and a hydroxyl group at position C2* to the kaempferol backbone. The 7-O-sulfate substituent has been found to be most efficient in homogenizing electron density over the entire three-ring skeleton, significantly reducing the electronic instability of transition-state geometry and hence increasing the IPT rate.

Acknowledgements

We are grateful to our parents for all supports and encouragement.

References

Alkhamees, O. A. (2013). Morin a flavonoid exerts antioxidant potential in streptozotocin-induced hepatotoxicity. *British Journal of Pharmacology and Toxicology 4*(1), 10-17.

Becke, A. D. (1993). Density-functional thermochemistry III. the role of exact exchange. *Journal of Chemical Physics*, *98*, 5648-5652.

Bondi, A. (1964). van der Waals Volumes and Radii. *Journal of Physical Chemistry*, *68*, 441-452.

Calderon-Montaño, J. M., Burgos-Moron, E., Perez-Guerrero, C., & Lopez-Lazaro, M. (2011). A review on the dietary flavonoid kaempferol. *Mini-Reviews in Medicinal Chemistry*, *11*(4), 298–344.

Chen, A. Y., & Chen, Y. C. (2013). A review of the dietary flavonoid, kaempferol on human health and cancer chemoprevention. *Food Chemistry*, *138*(4), 2099-2107.

Chen, Y.T., Zheng, R. L., Jia Z. J, & Ju, Y. (1990). Flavonoids as superoxide scavengers and antioxidants. *Free Radical Biology & Medicine, 9*(1), 19-21.

Doroshenko, A. O., Posokhov, E. A., Verezubova, A. A., & Ptyagina, L. M. (2000). Excited state intramolecular proton transfer reaction and luminescent properties of the ortho-hydroxy derivatives of 2,5-diphenyl-1,3,4-oxadiazole. *Journal of Physical Organic Chemistry*, *13*(5), 253-265.

Frisch, M. J., Trucks, G. W., Schlegel, H. B., Scuseria, G. E., Robb, M. A., Cheeseman, J. R., Scalmani, G., Barone, V., Petersson, G. A., Nakatsuji, H., Li, X., Caricato, M., Marenich, A. V., Bloino, J., Janesko, B. G., Gomperts, R., Mennucci, B., Hratchian, H. P., Ortiz, J. V., Izmaylov, A. F., Sonnenberg, J. L., Williams, Ding, F., Lipparini, F., Egidi, F., Goings, J., Peng, B., Petrone, A., Henderson, T., Ranasinghe, D., Zakrzewski, V. G., Gao, J., Rega, N., Zheng, G., Liang, W., Hada, M., Ehara, M., Toyota, K., Fukuda, R., Hasegawa, J., Ishida, M., Nakajima, T., Honda, Y., Kitao, O., Nakai, H., Vreven, T., Throssell, K., Montgomery Jr, J. A., Peralta, J. E., Ogliaro, F., Bearpark, M. J., Heyd, J. J., Brothers, E. N., Kudin, K. N., Staroverov, V. N., Keith, T. A., Kobayashi, R., Normand, J., Raghavachari, K., Rendell, A. P., Burant, J. C., Iyengar, S. S., Tomasi, J., Cossi, M., Millam, J. M., Klene, M., Adamo, C., Cammi, R., Ochterski, J. W., Martin, R. L., Morokuma, K., Farkas, O., Foresman, J. B., Fox, D. J., Gaussian 16 Revision B.01 (2016), Gaussian Inc., Wallingford CT.

Georgieva, I., Trendafilova, N., Aquino, A. J. A., & Lischka, H. (2007). Excited-state proton transfer in 7-hydroxy-4-methylcoumarin along a hydrogen-bonded water wire. *Journal of Physical Chemistry A*, *111*(1), 127–135.

Hirschfelder, J. O., & Wigner, E (1939). Some quantum-mechanical considerations in the theory of reactions involving an activation energy. *Journal of Chemical Physics*, *7*, 616–628.

Jacquemin, D., Perpète, E.A., Scuseria, G.E., Ciofini, I., & Adamo, C. (2008). TD-DFT performance for the visible absorption spectra of organic dyes: conventional versus long-range hybrids. *Journal of Chemical Theory and Computation*, *4*, 123-135.

Laidler, K. J., & King, M. C. (1983). Development of transition-state theory. *Journal of Physical Chemistry*, *87*(15), 2657-2664.

Lee, C., Yang, W., & Parr, R.G. (1988). Development of the Colle-Salvetti correlation-energy formula into a functional of the electron density. *Physical Review B*, 37, 785-789.

Marenich, A.V., Cramer, C.J., & Truhlar, D.G. (2009). Universal solvation model based on solute electron density and on a continuum model of the solvent defined by the bulk dielectric constant and atomic surface tensions. *Journal of Physical Chemistry B*, *113*, 6378-6396.

Markovic, Z., Milenkovic, D., Dorovic, J., Markovic, J. M. D., Stepanic, V., Lucic, B., & Amic, D. (2012). Free radical scavenging activity of morin 2′-O-phenoxide anion, *Food Chemistry, 135*, 2070–2077.

McMorrow, D., & Kasha, M. (1984). Intramolecular excited-state proton transfer in 3-hydroxyflavone: hydrogen-bonding solvent perturbations. *Journal of Physical Chemistry*, *88*(11), 2235–2243.

Panhwar, Q. K. & Memon, S. (2011). Synthesis and evaluation of antioxidant and antibacterial properties of morin complexes. *Journal of Coordination Chemistry*, 64, 2117-2129.

Parthasarathi, P., & Subramanian, V. (2006). Characterization of hydrogen bonding: from van der Waals interactions to covalency. In. Grabowski, S.J. (Ed.), *Hydrogen Bonding - New Insights*. (pp. 1-50). Dordrecht: Springer.

Pieniazek, E., Kalembkiewicz, J., Dranka, M., & Woznicka, E. (2014). Syntheses, crystal structures and antioxidant study of Zn(II) complexes with morin-5*-sulfonic acid (MSA). *Journal of Inorganic Biochemistry*, *141*, 180-187.

Sengupta, B., Reilly, S. M., Davis, D. E. Jr, Harris, K., Wadkins, R. M, Ward, D., Gholar, D., & Hampton, C. (2015). Excited state proton transfer of natural flavonoids and their chromophores in duplex and tetraplex DNAs. *Journal of Physical Chemistry B*, *119*(6), 2546-56.

Seyoum, A., Asres, K., & El-Fiky F. K. (2006). Structure–radical scavenging activity relationships of flavonoids. *Phytochemistry*, *67*(18), 2058-2070.

Suwattanamala, A., & Ruangpornvisuti, V. (2009). Isomeric structures of benzimidazole, benzoxazole, and benzothiazole derivatives, their electronic properties and transformations. *Structural Chemistry*, *20*, 619-631.

Yanai, T., Tew, D. P., & Handy, N.C. (2004). A new hybrid exchange–correlation functional using the Coulomb-attenuating method (CAM-B3LYP). *Chemical Physics Letter*, *393*, 51-57.

Yasarawan, N., Thipyapong, K., & Ruangpornvisuti, V. (2014). Exploring molecular structures, orbital interactions, intramolecular proton-transfer reaction kinetics, electronic transitions and complexation of 3-hydroxycoumarin species using DFT methods. *Journal of Molecular Graphics and Modelling*, *51*, 13-26.